Available online at www.sciencedirect.com
SCIENCE DIRECT®
Optics Communications 245 (2005) 355–361
OPTICS COMMUNICATIONS
www.elsevier.com/locate/optcom

Light transmission through a subwavelength microstructured aperture: electromagnetic theory and applications

Nicolas Bonod *, Evgeny Popov, Michel Nevière

Faculté des Sciences et Techniques de St. Jérôme, Institut FRESNEL, Unité Mixte de Recherche associée au Centre National de la Recherche Scientifique No. 6133, Université de Provence, Avenue Escadrille Normandie Niémen, 13397 Marseille Cedex 20, France

Received 29 July 2004; received in revised form 24 September 2004; accepted 15 October 2004

Abstract

A differential theory of diffraction by apertures and/or objects described in cylindrical coordinates is outlined. It projects the electromagnetic field on a Fourier–Bessel basis and uses correct rules to express the components of the electric displacement **D** on that basis which is truncated in view of numerical computation. Maxwell equations are then reduced to a finite first order differential set which provides a fast convergence of the results when the truncation order is increased. We apply the theory to the study of the transmission of a circular aperture inside a metallic screen connected with a tapered fiber. Coaxial devices can be studied as well.

PACS: 42.25.F
Keywords: Diffraction; Hole; Subwavelength

1. Introduction

After the discovery of the extraordinary light transmission by hole arrays [1] in 1998 and the great amount of theoretical and experimental work that it suggested, many researchers are trying to produce nano light sources by using a single subwavelength hole pierced in a metallic screen and increasing its natural light transmission by adding a circular corrugation, or a small concentric disk [2] to excite a new resonance or propagation process. Optimizing such a nano device requires Maxwell equations as a tool, while its geometry requires working in cylindrical coordinates. Our aim

* Corresponding author. Tel.: +33 491288824; fax: +33 491674428.
E-mail address: nicolas.bonod@fresnel.fr (N. Bonod).

0030-4018/$ - see front matter
doi:10.1016/j.optcom.2004.10.028

is to take advantage of the recent breakthrough of the differential theory in Cartesian coordinates [3,4] to develop a differential theory of diffraction in cylindrical coordinates able to analyze a wide class of microstructured devices, and giving results which converge fast when the truncation order of the field series is increased. The present method is thus an extension of the fast Fourier factorization (FFF) method [3,4], previously developed for objects periodic with respect to one or two Cartesian coordinates, to problems in which the field is represented at another kind of continuous function basis, namely a Bessel–Fourier basis. Such a generalization will be called fast numerical factorization (FNF).

2. Presentation of the theory

We assume a time harmonic dependence in $\exp(-i\omega t)$ so that Maxwell equations read:

$$\operatorname{curl}\mathbf{E}(\mathbf{r}) = i\omega\mu_0\mathbf{H}(\mathbf{r}), \tag{1}$$

$$\operatorname{curl}\mathbf{H}(\mathbf{r}) = -i\omega\mathbf{D}(\mathbf{r}) = -i\omega\varepsilon(\mathbf{r})\mathbf{E}(\mathbf{r}). \tag{2}$$

In cylindrical coordinates (r,θ,z) any object and field is periodic with respect to the polar angle θ, with period 2π, so that the field components can be represented on the $\exp(in\theta)$ basis. Moreover, as established in a previous work on waveguide theory [5], each Fourier component of the cylindrical components of the electric field can be expressed as an integral involving Bessel function $J_n(k_r r)$, where k_r is the r-component of the wavevector of each elementary spectral component of the field. Thus k_r continuously varies from 0 to ∞, but will be discretized into a set of values k_m, so that the field components finally read:

$$E_r(r,\theta,z) = i\sum_{n=-N}^{N}\sum_{m=1}^{\mathrm{Max}} k_m\Delta k_m\left[b^E_{n,m}(z)J_{n+1}(k_m r) - c^E_{n,m}(z)J_{n-1}(k_m r)\right]\exp(in\theta), \tag{3}$$

$$E_\theta(r,\theta,z) = \sum_{n=-N}^{N}\sum_{m=1}^{\mathrm{Max}} k_m\Delta k_m\left[b^E_{n,m}(z)J_{n+1}(k_m r) + c^E_{n,m}(z)J_{n-1}(k_m r)\right]\exp(in\theta), \tag{4}$$

$$E_z(r,\theta,z) = \sum_{n=-N}^{N}\sum_{m=1}^{\mathrm{Max}} k_m\Delta k_m E_{z,n,m}(z)J_n(k_m r)\exp(in\theta). \tag{5}$$

Similar equations apply to the cylindrical components of $\mathbf{H}$, with $b^E_{n,m}$ changed into $b^H_{n,m}$, $c^E_{n,m}$ into $c^{\mathrm{H}}_{n,m}$ and $E_{z,n,m}$ into $H_{z,n,m}$. Let us assume that the device has a cylindrical symmetry, i.e. that ε is θ-independent. Moreover, we assume it to be z-independent in a piecewise manner (Fig. 1), which enables us to use the eigenvalue/eigenvector method in integrating the differential set of equations. However, this does not represent a limitation of the method, because in the opposite case when ε varies with z, the system of equations can be integrated using some other numerical technique.

Eqs. (1) and (2) in cylindrical coordinates lead to the expression of the z-components of the electromagnetic field:

$$\sum_{m=1}^{\mathrm{Max}}(b^E_{n,m} - c^E_{n,m})J_n(k_m r)k_m^2\Delta k_m = i\omega\mu_0 H_{z,n}(r,z), \tag{6}$$

$$\sum_{m=1}^{\mathrm{Max}}(b^H_{n,m} - c^H_{n,m})J_n(k_m r)k_m^2\Delta k_m = -i\omega\varepsilon(r)E_{z,n}(r,z). \tag{7}$$

The problem which arises is to express the components of the product $\varepsilon(r)E_{z,n}(r,z)$ on the Bessel functions basis in terms of those of $\varepsilon(r)$ and

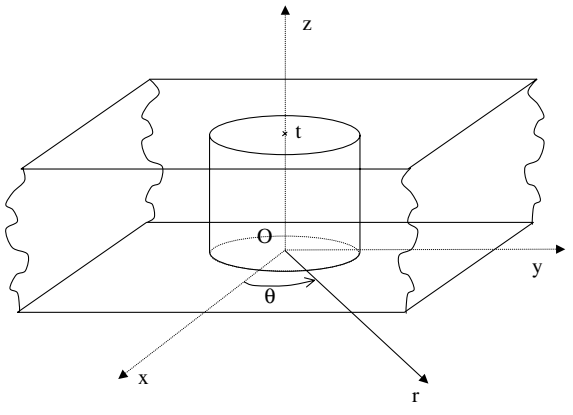

Fig. 1. Schematic representation of a diffraction system consisting of finite-length objects with cylindrical symmetry, surrounded by homogeneous media.

$E_{z,n}(r,z)$ a process that we call factorizing the product in the Fourier–Bessel basis. With the above-mentioned hypothesis, $E_z(r,\theta,z)$ is a field component tangential to the discontinuity surface and is thus continuous with respect to r. So are its Fourier components $E_{z,n}(r,z)$. Thus the Bessel components of the product can be obtained using the direct rule recently established in any continuous function basis [6]. We recall that if we consider three functions f, g, and h, such that $h = gf$, and f_p are the components of f on the φ_p function basis, then

$$h_m = \sum_p g_{mp} f_p, \tag{8}$$

where

$$g_{mp} = \langle g\varphi_p | \varphi_m \rangle. \tag{9}$$

Here we have to apply this rule to the (n)th Fourier components of $\varepsilon(r)$. As shown in [6], the (m,p)th Bessel components of g_n are given by

$$g_{n,mp} = \Delta k_m k_m \int_{r=0}^{\infty} r g_n(r) J_q(k_p r) J_{q'}(k_m r)\, \mathrm{d}r. \tag{10}$$

In this equation q and q' can be equal to (n), because E_z is expressed in term of the (n)th Bessel functions (see Eq. (7)); but q can also be equal to $(n+1)$ while q' is equal to $(n-1)$, and inversely, because, as shown in Eqs. (3)–(5), the (n)th Fourier components of E_r and E_θ are expressed in terms of the $(n+1)$th and $(n-1)$th Bessel functions. When applied to the function $\varepsilon(r)$, Eq. (10) allows computing a square matrix $[\varepsilon]^{n,\tilde{n}}$ having $(\mathrm{Max}+1)\times(\mathrm{Max}+1)$ size and with elements $[\varepsilon]^{n,\tilde{n}}_{p,m}$ defined by

$$[\varepsilon]^{n,\tilde{n}'}_{p,m} = k_m \Delta k_m \int_{r=0}^{\infty} \varepsilon(r) J_n(k_p r) J_{n'}(k_m r) r\, \mathrm{d}r. \tag{11}$$

The first subscript denotes the argument of the Bessel function with integer order written as the first superscript. m denotes the argument of the (n')th Bessel function and the tilda on n' indicates the presence of the term $k_m \Delta k_m$ in Eq. (11). Eq. (8) applied to Eq. (7) then leads to

$$k_m \left[b^H_{n,m} - c^H_{n,m} \right] = -\mathrm{i}\omega \sum_{m'=1}^{\mathrm{Max}} [\varepsilon]^{n,\tilde{n}}_{m,m'} E_{z,n,m'}. \tag{12}$$

Using matrix inversion, Eq. (12) gives the expression of $E_{z,n,m'}$ which can be substituted into Eq. (5) to lead to the following expression:

$$E_{z,n} = \sum_{m=1}^{\mathrm{Max}} \frac{\mathrm{i}k_m}{\omega} \Delta k_m J_n(k_m r) \times \sum_{m'=1}^{\mathrm{Max}} \left([\varepsilon]^{n,\tilde{n}} \right)^{-1}_{m,m'} k_{m'} \left[b^H_{n,m'} - c^H_{n,m'} \right]. \tag{13}$$

Differentiating Eqs. (3) and (4) gives

$$\frac{\mathrm{d}}{\mathrm{d}z}(E_{\theta,n} - \mathrm{i}E_{r,n}) = \sum_{m=1}^{\mathrm{Max}} 2k_m \Delta k_m \frac{\mathrm{d}b^E_{n,m}}{\mathrm{d}z} J_{n+1}(k_m r) \tag{14}$$

and Maxwell equations lead to

$$\frac{\mathrm{d}}{\mathrm{d}z}(E_{\theta,n} - \mathrm{i}E_{r,n}) = -\mathrm{i}\omega\mu_0 H_{r,n} - \mathrm{i}\frac{\partial E_{z,n}}{\partial r} + \omega\mu_0 H_{\theta,n}. \tag{15}$$

By replacing all field components by their Fourier series, using the differentiation relations of Bessel functions, multiplying both members by $J_{n+1}(k'_m r)$ and integrating from to 0 to ∞, we obtain, due to the orthogonality of Bessel functions

$$\frac{\mathrm{d}\tilde{b}^E_{n,m}}{\mathrm{d}z} = \omega\mu_0 \tilde{b}^H_{n,m} - \frac{k_m}{2\omega} \times \sum_{m'=1}^{\mathrm{Max}} \left([\varepsilon]^{\tilde{n},n} \right)^{-1}_{m,m'} k_{m'} \left[\tilde{b}^H_{n,m'} - \tilde{c}^H_{n,m'} \right], \tag{16}$$

where $\tilde{b}^E_{n,m} = k_m b^E_{n,m}$, $\tilde{b}^H_{n,m'} = k_{m'} b^H_{n,m'}$, $\tilde{c}^H_{n,m'} = k_{m'} c^H_{n,m'}$. The term $\mathrm{d}\tilde{b}^H_{n,m}/\mathrm{d}z$ is calculated in a similar way, except that since it involves the continuous product $\varepsilon(r)E_{r,n}(r,z)$ of discontinuous functions, the inverse rule stated in [6] has to be used.

Finally, we also derive $\mathrm{d}\tilde{c}^E_{n,m}/\mathrm{d}z$ and $\mathrm{d}\tilde{c}^H_{n,m}/\mathrm{d}z$ along the previous lines, so that Maxwell equations are written as a set of $(2N+1)$ first-order differential equations, which can be written in matrix form

$$\frac{\mathrm{d}\mathbf{F}_n(z)}{\mathrm{d}z} = M_n \mathbf{F}_n(z), \tag{17}$$

with $n \in [-N,N]$. In this equation, each $\mathbf{F}_n$ is a column-vector made of four blocks containing the Bessel components $\tilde{b}^E_{n,m}$, $\tilde{c}^E_{n,m}$, $\tilde{b}^H_{n,m}$, $\tilde{c}^H_{n,m}$ which means that $\mathbf{F}_n$ has $4(\mathrm{Max}+1)$ components; M_n are $4(\mathrm{Max}+1)\times 4(\mathrm{Max}+1)$ square matrices whose

elements are obtained by Eq. (16) and similar equations for $\tilde{c}^{E}_{n,m}, \tilde{b}^{H}_{n,m}$, and $\tilde{c}^{H}_{n,m}$, not written here. For any value of n, the M_n-matrix can be represented in a block form:

$$M_n = \begin{pmatrix} M_{n,11} & M_{n,12} \\ M_{n,21} & M_{n,22} \end{pmatrix}, \tag{18}$$

where blocks $M_{n,ij}$ are given by:

$$\begin{aligned}
M_{n,11} &= 0, \\
M_{n,12} &= \begin{pmatrix} -\frac{1}{2\omega}K\left[\varepsilon^{\tilde{n},n}\right]^{-1}K + \omega\mu_0 I & -\frac{1}{2\omega}K\left[\varepsilon^{\tilde{n},n}\right]^{-1}K \\ -\frac{1}{2\omega}K\left[\varepsilon^{\tilde{n},n}\right]^{-1}K & \frac{1}{2\omega}K\left[\varepsilon^{\tilde{n},n}\right]^{-1}K - \omega\mu_0 I \end{pmatrix}, \\
M_{n,21} &= \begin{pmatrix} \frac{K^2}{2\omega\mu_0}I - \frac{\omega}{2}\left(\left[\widetilde{\frac{1}{\varepsilon}}^{n+1,n+1}\right]^{-1} + \left[\widetilde{\varepsilon}^{n+1,n+1}\right]\right) & -\frac{K^2}{2\omega\mu_0}I + \frac{\omega}{2}\left(\left[\Psi\right]^{\widetilde{n+1,n-1}}\left[\widetilde{\frac{1}{\varepsilon}}^{n-1,n-1}\right]^{-1} - \left[\widetilde{\varepsilon}^{n+1,n-1}\right]\right) \\ \frac{K^2}{2\omega\mu_0}I - \frac{\omega}{2}\left(\left[\Psi\right]^{\widetilde{n-1,n+1}}\left[\widetilde{\frac{1}{\varepsilon}}^{n+1,n+1}\right]^{-1} - \left[\widetilde{\varepsilon}^{n-1,n+1}\right]\right) & -\frac{K^2}{2\omega\mu_0}I + \frac{\omega}{2}\left(\left[\widetilde{\frac{1}{\varepsilon}}^{n-1,n-1}\right]^{-1} + \left[\widetilde{\varepsilon}^{n-1,n-1}\right]\right) \end{pmatrix}, \\
M_{n,22} &= 0,
\end{aligned} \tag{19}$$

with

$$\left[\Psi\right]^{\widetilde{n-1,n+1}}_{m,m''} = k_m \Delta k_m \int_{r=0}^{\infty} J_{n-1}(k_m r) J_{n+1}(k_{m''} r) r \, \mathrm{d}r. \tag{20}$$

As in Eq. (11), m denotes the argument of the $(n-1)$ Bessel function, and the tilda on $(n-1)$ indicates the presence of $k_m \Delta k_m$ in Eq. (20). The integration of Eq. (17) is done using the eigenvalue–eigenvector technique since ε is assumed to be z-independent. The resolution of the boundary-value problem through a shooting method provides the field everywhere, once the field incident from one side in the surrounding homogeneous media $z \to \pm\infty$ is given.

3. Numerical calculation: light coupling and propagation in a glass fiber

In order to demonstrate the possibilities of the method, we have chosen a numerical example involving several physical phenomena and introducing difficulties for the modelization by studying a system that has both metallic and dielectric parts (Fig. 2). It consists on a metallic (silver) screen with a circular hole in it. The linearly polarized incident plane wave falls with unit amplitude normally on the screen from the superstrate made of air with refractive index $n = 1$. A glass fiber (refractive index 1.5) is stuck in the hole and continues in the air below the screen. The wavelength is $\lambda = 0.5$ μm. When the incident light hits the screen (having 0.2 μm thickness), it is reflected back and the transmission through the screen can be neglected. Due to the hole with a fiber end in it, a part of the incident light is coupled through the hole into the fiber. The fiber radius is small enough ($R = 0.125$ μm) to cut off all the fiber modes except the fundamental mode HE_{11} [5]. Due to that fact, far enough below the screen, all transition fields due to the diffraction by the upper and lower boundaries of the hole are attenuated and one can expect to observe only the propagating mode. And indeed, Fig. 3 shows that almost all the energy of the electric field is concentrated inside the fiber. There is practically no difference in the field distribution and amplitude when the distance h between the screen and the measuring point is, say, 50λ or 100λ, as shown in the figure. The sharp peaks at the surface of the fiber are due to the discontinuity of the radial component of the electric field, as discussed further in the text.

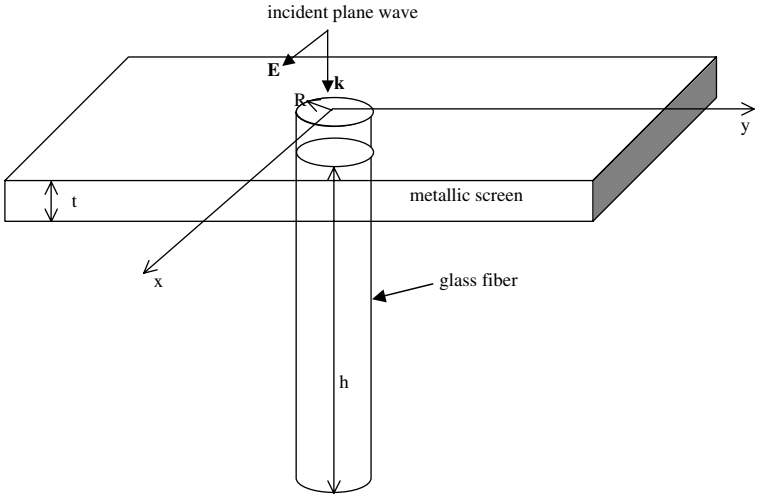

Fig. 2. Glass fiber stuck into metallic screen hole illuminated in normal incidence from above by an linearly polarized plane wave (electric field vector parallel to the x-axis), with unit amplitude.

The results given in Fig. 3 were obtained by truncating the sums in Eqs. (3)–(7) to Max = 700 and using $\Delta k_m = 0.0007\ \mathrm{nm}^{-1}$. The main problem in the numerical modeling of diffraction is the convergence of the method with respect to the number of equations and its precision stability when replacing the integral representation by finite sums. Fig. 4 shows the convergence of the method with respect to the maximum wavenumber $k_{r,\mathrm{Max}} = \Delta k_m \times \mathrm{Max}$ along the r-axis, i.e. the truncation of the basis, normalized with respect to the incident wavenumber k_0. As can be observed, without correctly applying the direct and the inverse factorization rules, the amplitude of the guided mode fluctuates strongly when $k_{r,\mathrm{Max}}$ is varied, while the correct application of the rules (with the FNF method) gives reliable result for $k_{r,\mathrm{Max}}/k_0 \geqslant 20$, which, for numerical applications, corresponds to a quite reasonable value of Max = 180 when $\Delta k_m = 0.0007\ \mathrm{nm}^{-1}$. The latter value is small enough to observe no change when

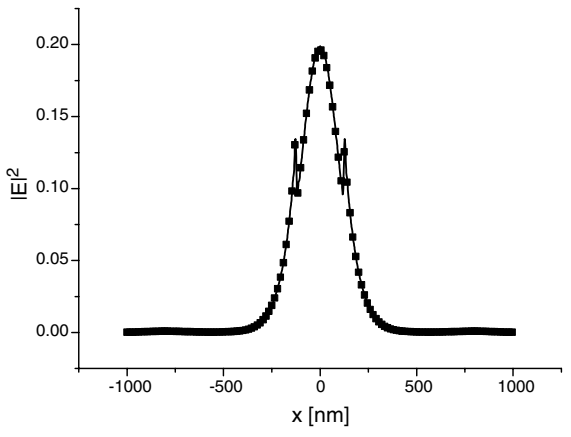

Fig. 3. Squared modulus of the electric field at a distance $h = 25$ μm (squares) and 50 μm (full line) from the metallic screen, representing the fundamental mode excited by the incident plane wave and propagating inside the fiber ($R = 0.125$ μm).

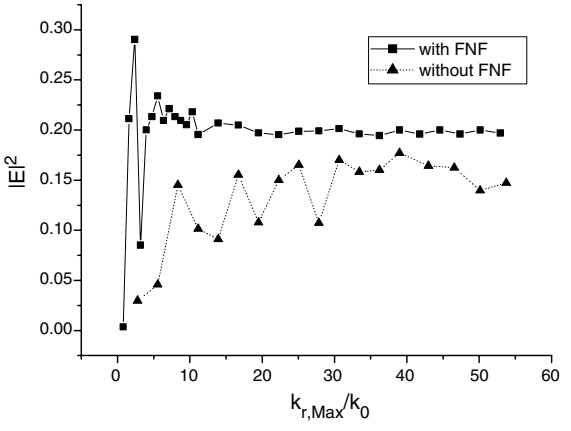

Fig. 4. Convergence of the value of $|E|^2$, calculated on the axis of the fiber at a distance $h = 50$ μm after the screen, as a function of the truncation of the radial wavenumber component in the Fourier–Bessel representation. Squares, with FNF, triangles, without FNF.

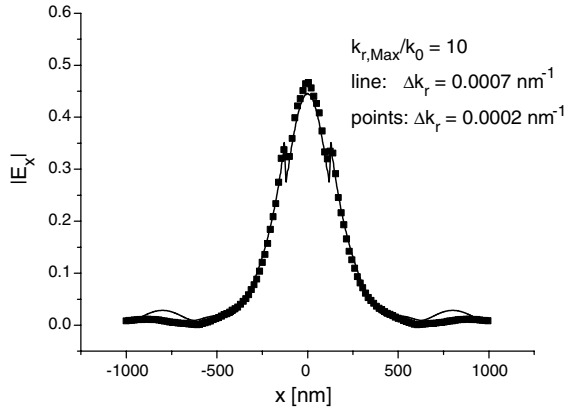

Fig. 5. Variation of the radial component of the electric field along the x-axis for two different values of Δk_m given in the figures in units of nm^{-1} and calculated at $h = 50$ μm.

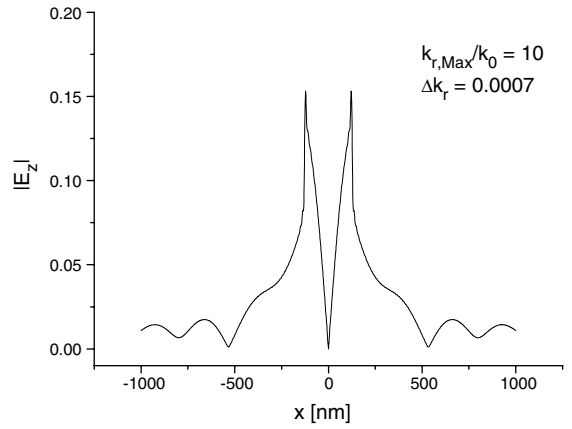

Fig. 6. Radial variation of the longitudinal electric field component for $h = 50$ μm.

$\Delta k_m = 0.0007$ nm^{-1} is reduced further by keeping $k_{r,\mathrm{Max}}/k_0$ fixed. This fact is demonstrated in Fig. 5, where the electric field component perpendicular to the fiber surface presents a sharp discontinuity, contrary to the longitudinal component E_z, which is continuous across the fiber boundaries (Fig. 6).

4. Comparison with other results: light diffraction by a single hole

Unfortunately, in the literature there are not many quantitative results for the distribution of the field through a single circular aperture to be used in order to directly compare with our method. We have chosen a recently published paper by Yin et al. [7]. The authors compare experimental and theoretical results of the field diffracted by a hole with a radius 100 nm pierced in a 100 nm Au film deposited on a fused quartz substrate for 532 nm wavelength of linearly polarized light incident from the substrate side. They find that the major contribution in the x-component of the diffracted field comes from a plasmon-like surface wave propagating away from the hole. The measured field intensity at a distance 5 nm above the film surface has a well-pronounced quasiperiodicy with a period approximately equal to 471 nm. The results taken from Fig. 2 of [7] at normal incidence are shown with squares in Fig. 7. We have made the same calculations with Au complex refractive index equal to 0.33 + i2.05. This index value corresponds to a plasmon surface wave propagating on air–Au interface with a normalized propagation constant $\tilde{\alpha}_g \equiv k_r/k_0 \approx 1.1275 + \mathrm{i}0.0528$. At 532 nm this constant corresponds to a wave with a period $D = \lambda/Re(\tilde{\alpha}_g) \approx 571.8$ nm. The results of our method are plotted with a solid line. They represent the normalized intensity calculated according to the formula $c\left(|E_x|^2 - I_0\right)/\sqrt{x}$, used in [7], where I_0 is the value measured far away from the hole (equal to 0.02 times the incident field intensity in our results) and $c = 0.5$ in order to fit the two

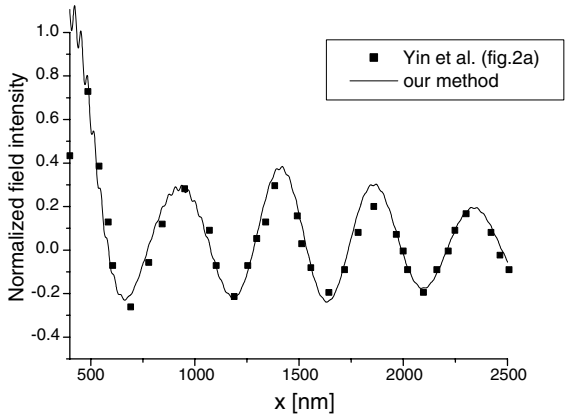

Fig. 7. Normalized intensity of the x-component of the field $0.5(|E_x|^2 - 0.02|E_{\mathrm{incident}}|^2)/\sqrt{x}$, see the text for details. Squares, data scanned from Fig. 2 of [7], solid line, our results.

curves (the results in [7] are in arbitrary units). The comparison starts at about half a wavelength from the hole boundaries, because at nearer vicinity the field fluctuations have much larger amplitude. As one can observe, our results present the same type of quasiperiodicy having the same period as in [7] (471 nm) and approximately equal to the expectations from the simple model based on plasmon wave excitation.

5. Conclusions

A new rigorous electromagnetic method is developed, which extends the differential formalism well known for modeling light diffraction by periodic systems to model finite-length cylindrical objects having rotational symmetry. The method is suitable for studying light diffraction by dielectric or metallic cylinders with finite length, by circular single or structured hole. It can be successfully applied to fiber coupling and fiber-end diffraction. The convergence of the method with respect to the number of radial wave components is ensured by applying specific factorization rules valid in a truncated basis of continuous functions.

References

[1] T.W. Ebbesen, H.J. Lezec, H.F. Ghaemi, T. Thio, P.A. Wolff, Nature 391 (1998) 667.
[2] A. Moreau, G. Granet, F.I. Baida, D. VanLabeke, Opt. Express 11 (2003) 1131.
[3] E. Popov, M. Nevière, J. Opt. Soc. Am. A 18 (2001) 2886.
[4] M. Nevière, E. Popov, Light Propagation in Periodic Media; Differential Theory and Design, Marcel-Dekker, New York, Basel, Honk Kong, 2003.
[5] A. Snyder, J.D. Love, Optical Waveguide Theory, Chapman and Hall, London, New York, Tokyo, Melbourne, Madras, 1983, p. 250.
[6] E. Popov, M. Nevière, N. Bonod, J. Opt. Soc. Am. A 21 (2004) 46.
[7] L. Yin, V. Vlasko-Vlasov, A. Rydh, J. Pearson, U. Welp, S. Chang, S. Gray, G. Scharz, D. Brown, C. Kimball, Appl. Phys. Lett. 85 (2004) 467.